Proceedings of the 2005 IEEE
Engineering in Medicine and Biology 27th Annual Conference
Shanghai, China, September 1-4, 2005

Imaging Breathing Rate in the CO_2 Absorption Band

Jin Fei
Department of Computer Science
University of Houston
Houston, Texas 77204–3010
jinfei@cs.uh.edu

Zhen Zhu
Department of Computer Science
University of Houston
Houston, Texas 77204–3010
zhu@cs.uh.edu

Ioannis Pavlidis
Department of Computer Science
University of Houston
Houston, Texas 77204–3010
ipavlidi@central.uh.edu

Abstract— **Following up on our previous work, we have developed one more non-contact method to measure human breathing rate. We have retrofitted our Mid-Wave Infra-Red (MWIR) imaging system with a narrow band-pass filter in the CO_2 absorption band ($4.3\ \mu m$). This improves the contrast between the foreground (i.e., expired air) and background (e.g., wall). Based on the radiation information within the breath flow region, we get the mean dynamic thermal signal. This signal is quasi-periodic due to the interleaving of high and low intensities corresponding to expirations and inspirations respectively. We sample the signal at a constant rate and then determine the breathing frequency through Fourier analysis. We have performed experiments on 9 subjects at distances ranging from $6-8\ ft$. We compared the breathing rate computed by our novel method with ground-truth measurements obtained via a traditional contact device (PowerLab/4SP from ADInstruments with an abdominal transducer). The results show high correlation between the two modalities. For the first time, we report a Fourier based breathing rate computation method on a MWIR signal in the CO_2 absorption band. The method opens the way for desktop, unobtrusive monitoring of an important vital sign, that is, breathing rate. It may find widespread applications in preventive medicine as well as sustained physiological monitoring of subjects suffering from chronic ailments.**

I. Introduction

Human breathing consists of expiring air rich in CO_2 and inspiring air rich in O_2 to maintain vital functions. Breath analysis plays an important role in the diagnosis and management of respiratory diseases like sleep obstructive apnea and asthma. In fact, breathing rate is one of the vital signs and hence, indicative of the overall health status of a subject. The normal breathing rate of resting adults varies from $12-18$ cycles per minute (cpm) [1].

Various types of contact modalities have been developed to measure human breathing rate. Iamratanakul et al. [2] studied the correlation of breathing and heart rates based on sinus arrhythmia. They estimated the breathing signal by demodulating arterial blood pressure. McNames et al. [3][4] analyzed abnormal breathing via the Electro-Cardio-Gram (ECG).

The respiratory belt transducer [5], measures the breathing rhythm via pressure changes on the strap sensor fitted on the subject's chest. This is rather uncomfortable to subjects and sensitive to motion.

All the aforementioned methods are contact methods and require the subject's cooperation. The first non-contact breathing rate measurement method was introduced by Greneker et al. [6] and based on active sensing. It is called Radar Vital Signs Monitor (RVSM) and is able to measure the subject's heart beat and breathing rate at distances up to $30\ ft$. It senses the chest wall moving up and down during breathing by Doppler modulated radar. The RVSM measurements are sensitive to small body movement.

Thermal infrared imaging is a passive contact-free modality. In previous publications we have demonstrated that thermal imaging can be used to measure various physiological variables, including blood flow [7], heart rate [8], and breathing rate [9]. In fact, it is an ideal modality for sustained physiological monitoring [10].

In [9] we have proposed a statistical methodology that models breathing as a mixture of expiration and non-expiration distributions. Every frame is classified as expiratory or non-expiratory by comparing the incoming distributions with the existing distributions using the Jeffrey's divergence measure. Thanks to this frame labelling we are able to compute the breathing rate.

In this paper, we introduce a Fast Fourier Transform (FFT) based method to estimate human breathing rate through thermal video sequences. This is an alternative to the statistically-laden approach we reported previously. It is based on the quasi-periodic nature of the breathing signal and not its bi-modality. In section II we describe the filtration of the thermal signal through an optical filter tuned to the CO_2 absorption band ($4.3\ \mu m$). This is a new acquisition method meant to boost the relative power of the breathing signal in the thermal imagery. In section III we outline our tracking method, the selection of regions of interest, and other data preprocessing. In section IV we describe a novel method to apply multi-stage FFT on the signals. We discuss our experimental setup and results in sections V and VI, respectively. Section VII concludes the paper.

II. Optical Filtering in the CO_2 Absorption Band

The breath thermal signal is very weak and of transient nature [9]. In an effort to improve the Signal to Noise ratio (S/N) we filter the MWIR radiation passing through the lens of our camera system with an optical filter tuned in the CO_2 absorption band ($4.3\ \mu m$). In this narrow band two natural mechanisms work to the benefit of our cause:

- **Atmospheric Transmittance.** Fig. 1 shows the atmospheric transmittance of infrared radiation at a distance of $30\ ft$ [11]. The diagram shows significant transmittance attenuation around $4.3\ \mu m$, which is due to

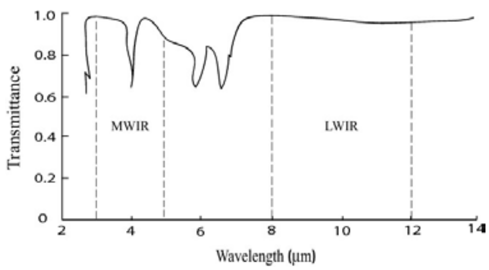

Fig. 1. Atmospheric transmittance of infrared radiation at a distance of 30 ft.

radiation absorption by CO_2 molecules. This attenuation depends on path length and grows larger for longer paths, while it is smaller for shorter paths. In our case, the background (e.g., wall) radiation has to travel longer distance to the sensor with respect to the breath and therefore, it is attenuated more.

- **$\mathbf{CO_2}$ Concentration.** The expired air from the human nasal cavity has slightly higher temperature and substantially higher CO_2 density (3.7%) than the ambient air (0.04%) [1]. The high density cluster of CO_2 molecules absorb monochromatic radiation at $4.3\ \mu m$ emitted from the background (e.g., wall) and boost the thermal power of the breath in this band even further.

The end result is increased contrast in the thermal imagery between weakened background and boosted breath intensities. This discriminating feature provides the basis for the development of our method.

Fig. 2 (a) shows a thermal snapshot of a subject during the inspiration phase. One can observe the uniform intensity background around the nasal area due to the absence of "hot" expired air, rich in CO_2. Fig. 2 (b) shows a thermal snapshot of a subject during the expiration phase. One can observe the contrast between the higher intensity expired air, next to the nasal area and the lower intensity surrounding background. This contrasting feature appears during expiration and disappears during inspiration. Therefore, it is a signature that characterizes the human breathing cycle and can enable measurement of the breathing rate. Fig. 2 (c) shows the color-map used in the images of Fig. 2 (a) and (b).

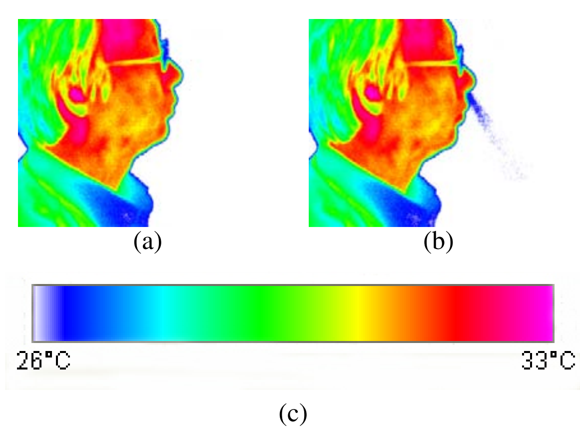

Fig. 2. (a) Inspiration phase. (b) Expiration phase. (c) Color-map.

III. Preprocessing

All subjects in our video clips are mostly stationary and exhibit only occasional minor movement. To overcome the inaccuracy caused by such movement, we use a simple tracker. We assume that the displacement of the head is small compared to the size of the image. We choose the nasal tip as the Tracking Region of Interest (TROI) (see Fig. 3). This area marks the beginning of the stream of expired air and at the same time provides excellent contrast (tissue versus background) for tracking purposes. Our tracking method is based on the iterative image registration technique [12].

We select as the Measurement Region of Interest (MROI) an area just below the tip of the nose and up to the level of the mouth, where we expect the expired stream of air to flow through (see Fig. 3). We compute the mean temperature within the MROI in each frame. Along the timeline, this produces a quasi-periodic temperature signal, which is indicative of the breathing function.

The video sampling rate fluctuates around 55 frames per second (fps). Considering that breath is a low frequency physiological process, we find that a lower sampling rate suffices for our computation (see Fig. 4). This does not only provide us a constant sampling rate, but also decreases computational time complexity. Experimentally, we chose $10\ fps$ as the re-sampling rate of the temperature signal.

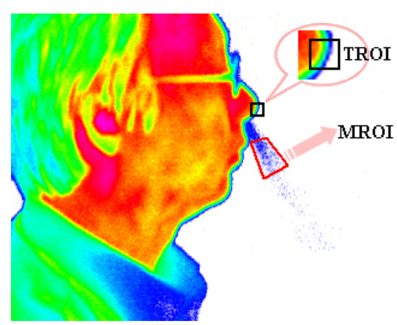

Fig. 3. The Tracking Region of Interest (TROI) is depicted as a small dark rectangle at the tip of the nose. The Measurement Region of Interest (MROI) is depicted as a polygon next to the nasal-mandibular region.

IV. Methodology

The breathing thermal signal, as the pulse thermal signal [7], is quasi-periodic in nature. Therefore, it can be analyzed through Fourier transformation. Since we operate on the discrete domain we use the Fast Fourier Transform (FFT). The FFT algorithm was introduced by Cooley et al. [13]. It approximates the continuous Fourier transform with great accuracy [14].

We perform FFT analysis on sliding segments (windows) of the normalized breathing thermal signal. From the resulting power spectra we remove responses corresponding to frequencies outside the range $[5 - 40]\ cpm$. We consider frequencies outside this range unlikely to occur in our experimental scenarios (healthy individuals at rest or undergoing mild aerobic exercise). We select the dominant frequency in the power spectrum of each sliding window as the likely

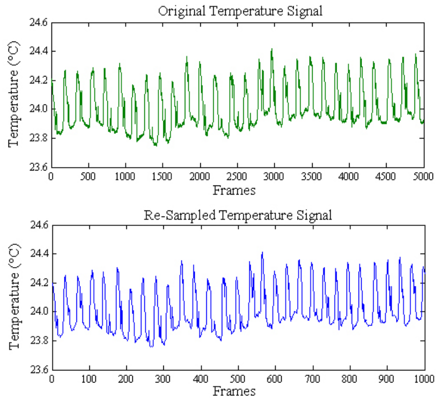

Fig. 4. Original and re-sampled temperature signals from the MROI of a subject. One can observe that the shapes of the signals are very similar, although the respective time scales are radically different.

breathing rate at the time. Fig. 5 illustrates the major steps of our methodology.

We define as $\mathbf{V}_i[t],\ t \in [0 \cdots N]$, the down-sampled breathing temperature signal framed in sliding window i. We normalize the signal $\mathbf{V}_i[t]$ as follows:

$$\mathbf{V}'_i[t] = \frac{\mathbf{V}_i[t] - \mu_i}{\sigma_i}, \tag{1}$$

where μ_i and σ_i are the mean and standard deviation of $\mathbf{V}_i[t]$ respectively. The normalization transforms signal $\mathbf{V}_i[t]$ to $\mathbf{V}'_i[t]$ that features mean $\mu'_i = 0$ and standard deviation $\sigma'_i = 1$ (see Fig. 5 (a)).

We apply FFT on the autocorrelation sequence $\phi_{\mathbf{V}'_i\mathbf{V}'_i}[t]$ of signal $\mathbf{V}'_i[t]$, to compute the power density spectrum:

$$\Phi_{\mathbf{V}'_i\mathbf{V}'_i}(e^{j\omega}) = \sum_{t=-\infty}^{\infty} \phi_{\mathbf{V}'_i\mathbf{V}'_i}[t] e^{-j\omega t} \tag{2}$$

In Fig 5 (b), we present the power spectrum density of signal $\mathbf{V}'_i[t]$ that corresponds to the window ending in frame $t = 2024$. The cut-off lines exclude the portion of the power spectrum that corresponds to uninteresting frequencies (outside the $[5-40]$ cpm range). The dominant frequency of 18.16 cpm is indicated in the diagram.

We adjust the size of the window as the timeline evolves. Initially, the window size is small, but then it expands as time permits. The goal is to start reporting breathing rate as soon as possible, while incrementally improving the computational accuracy over time.

Sliding window $i = 1$ applies to the normalized signal $\mathbf{V}'_1[t],\ t \in [0 \cdots N_1]$. We set $N_1 = 2^8 = 256$ samples, which means that breathing rate is reported for the first time after $25.6 sec$, since the down-sampled frame rate is 10 fps. After that, breathing rate is reported every 0.1 sec, as the window slides one sample to the right with every incoming frame. The window maintains the size N_1, until the total number of processed frames becomes $N_2 = 2 * N_1 = 2^9 = 512$, which is the next power of two. Then, it automatically adjusts to the larger power size. The size of the window adjusts one final time when the total number of processed frames reaches $N_3 = 2 * N_2 = 2^{10} = 1024$ and retains this value for the remaining monitoring period. Therefore, the method achieves top accuracy after 102.4 sec of operation.

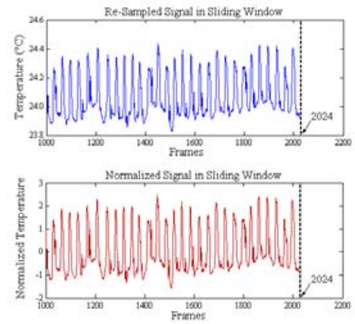

(a)

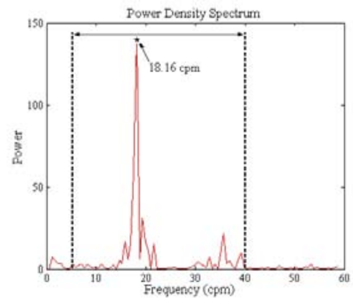

(b)

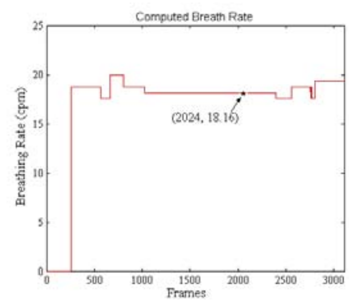

(c)

Fig. 5. Computational steps.(a) Normalization of windowed signal. (b) Power density Spectrum. (c) Breathing rate.

V. Experimental Setup

The experimental setup is composed of three devices: (a) Automatic THErmal Monitoring System (ATHEMOS), (b) Ground-Truth System (GTS), and (c) Electronic Trigger (ET).

A. ATHEMOS

ATHEMOS is the centerpiece of the experimental setup and performs the imaging operation. It is composed of the following items:

- An Indigo Phoenix Mid-Wave Infra-Red (MWIR) camera with an Indium Antimonite (InSb) detector operating in the range $3-5$ μm [15].
- A MWIR $50mm$ lens $f/2.3$, $Si : Ge$, bayonet mount from Indigo Systems [15].

- A pan-tilt head (model $QPT-90/1301C$) $150lb$ capacity from Quickset [16].
- A Model 2004, $4''$ differential black body from Santa Barbara Infrared for accurate system calibration [17].
- A DELL Precision 650 workstation that controls the setup and performs the algorithmic processing [18].
- A DELL cart that houses all the equipment.

The MWIR camera has a focal plane array (FPA) with maximum resolution of 640×512 pixels and a maximum sampling rate of 120 fps. The sensitivity is $0.025°$ C. The camera mounts on the pan-tilt, which serves as the positioning mechanism. It pans up to $435°$ and tilts up to $\pm 90°$.

A narrow band-pass optical filter from Spectrogon [19] is attached between the camera's FPA and lens. The center wavelength of the filter is 2343.5 cm^{-1} or 4269 nm, which is close to the absorption wavelength of the fundamental vibration of CO_2 molecules. In Fig. 6, one can observe that the 5% cutoff wavelengths of the filter are 2421.2 cm^{-1} (4130.2 nm) and 2259 cm^{-1} (4426.7 nm) respectively.

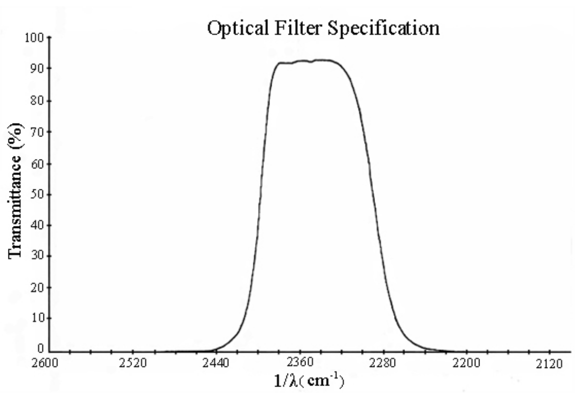

Fig. 6. Transmittance of band-pass filter used in ATHEMOS.

B. GTS

The GTS is composed of the following items:

- A ML750 PowerLab/4SP data acquisition system from ADInstruments [5].
- A MLT1132 respiratory belt transducer from ADInstruments [5]

The PowerLab/4SP has four channels, one of which connects to the respiratory belt transducer. The transducer fits around the subject's chest wall. By measuring the up and down movement of the thoracic cavity, the sensor forms the signal and sends it to the computer. The sampling rate is 100 samples per sec.

C. ET

The trigger connects to PowerLab/4SP via the BNC trigger port and interfaces to the Dell workstation via the parallel port. The trigger activates ATHEMOS and GTS simultaneously.

All the above subsystems integrate into a highly automated system, controlled by our user-friendly software. Fig. 7 (a) depicts the full experimental setup when the system is used in clinical trial mode. Fig. 7 (b) depicts the desktop setup when the system is used in application mode. In our clinical trials the subject is located $6-8$ ft away from the system and offers a profile view. The experiments take place in a dimly lit, climate controlled room. The subject is also fitted with the respiratory belt transducer, to ground truth the imaging measurements. The trigger in cooperation with custom software synchronize and record both the imaging and ground-truth signal information. The MWIR camera has been calibrated with a two-point calibration at $28°$ C and $38°$ C, which are the end points of a typical temperature distribution on a subject's face. The video recording speed is set at 55 fps.

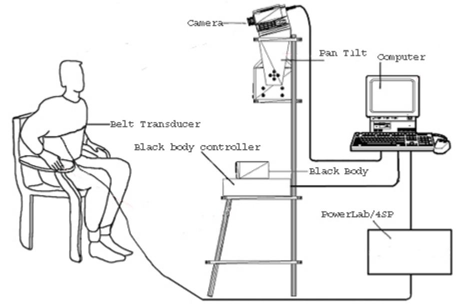

(a)

(b)

Fig. 7. (a) Schematic of clinical experimental setup. (b) Schematic of desktop setup.

VI. Experimental Results

We have recorded nineteen (19) thermal clips of nine (9) subjects. Seventeen (17) of the clips were recorded while the subjects were at rest. The remaining two (2) clips were recorded after the subjects undergone 2 min of moderate aerobic exercise. For many subjects we have recorded more than one clip at different times. All the thermal clips are 5 min in length.

Table I shows the detailed experimental results for all the thermal clips and all three windowing stages of the FFT based computation. The imaging results are juxtaposed with the corresponding ground-truth measurements obtained through the respiratory belt transducer.

We can observe that the imaged breath rate in stage 3 is closer to ground-truth than that in stages 2 and 1. In turn, the imaged breath rate in stage 2 is more accurate than that in stage 1. The breath rates corresponding to clips D005-016 and D005-019 are higher, since these clips were recorded after the subjects undergone moderate aerobic exercise.

TABLE I

GROUND-TRUTH VERSUS IMAGED BREATH RATE COMPARISON

Clip ID	Length	Stage 1[a]		Stage 2		Stage 3	
	(sec)	GBR[b]	IBR[c]	GBR	IBR	GBR	IBR
D005-007	302.60	19.67	18.75	15.73	17.71	16.50	17.28
D005-008	302.60	7.96	11.30	6.74	7.64	4.96	5.39
D005-010	300.80	13.89	16.53	14.73	15.23	11.69	13.27
D005-012	304.00	13.57	15.08	15.96	16.34	14.12	14.81
D005-016	300.80	37.16	37.50	32.03	34.65	27.10	28.97
D005-017	302.20	14.17	11.93	10.83	10.00	9.02	8.82
D005-019	315.60	26.68	27.06	21.79	24.23	21.11	21.20
D005-021	306.70	20.43	22.03	20.77	20.75	24.28	24.81
D005-022	310.40	16.44	18.75	18.11	18.85	17.78	18.33
D005-023	305.40	4.76	7.80	9.42	8.61	7.52	7.74
D005-024	305.90	10.86	12.45	10.93	11.81	11.92	12.03
D005-026	307.00	14.93	16.40	15.54	16.40	15.99	16.37
D005-027	305.20	19.83	21.09	20.38	21.00	19.91	21.43
D005-028	306.32	16.59	18.75	17.33	17.69	14.63	16.06
D005-029	305.40	16.90	18.88	16.87	17.72	13.60	15.31
D005-033	360.80	19.91	23.43	21.34	22.65	21.04	20.05
D005-037	401.00	4.41	7.82	4.64	5.98	6.40	5.99
D005-038	306.20	16.00	18.75	13.95	15.84	12.20	13.30
D005-039	325.60	10.91	14.06	10.30	11.96	10.79	10.98

[a]Breath rate unit is cycles/min
[b]Ground-Truth Breath Rate
[c]Imaged Breath Rate

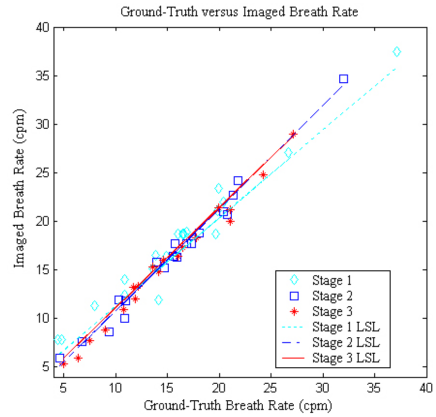

Fig. 8. Linear correlation of Ground-Truth Breath Rate and Imaged Breath Rate. Stage 1: $R = 0.9810$, $p = 1.52E - 013$; Stage 2: $R = 0.9895$, $p = 1.52E - 016$; Stage 3: $R = 0.9906$, $p = 3.68E - 017$.

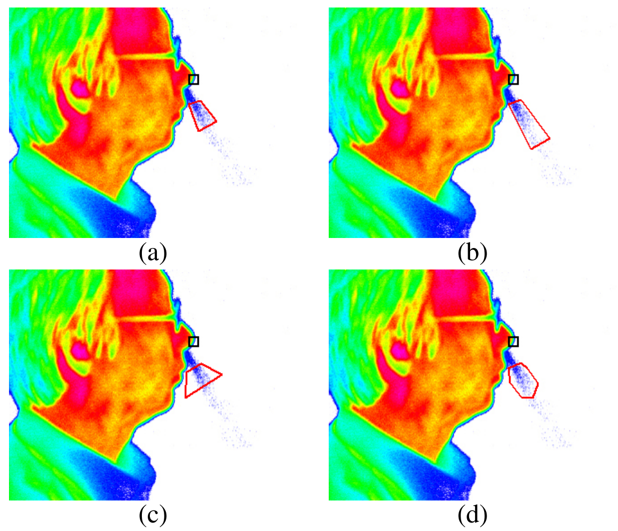

Fig. 9. MROIs of different shapes and sizes used in sensitivity analysis for clip D005-010.

We use the Pearson product measurement R [20] to evaluate the linear correlation between the imaged breath rate (Y) and the ground-truth breath rate (X). The higher the value of R, the stronger the correlation of X and Y is. We also compute the p-value to test the hypothesis of no correlation. If the p-value is small, normally less than 0.05, then the correlation R is significant. Fig. 8 illustrates the linear correlation of ground-truth and imaged breath rate, based on the results listed in Table I.

The breath rates from the two modalities are highly correlated in stage 3, with $R = 0.9906$ and $p = 3.68E-017$. Even in stages 1 and 2 the correlation is strong, but not as strong as in stage 3. Thus, by applying multi-stage FFT analysis on the breath temperature signal, we obtain greater accuracy as the window size increases.

To assess the sensitivity of our method to the shape and size of MROI we selected randomly a video clip from our set (D005-010). Then, we applied our computational methodology on MROIs of different shape and size for this particular clip (see Fig. 9). The experimental results are shown in Table II and demonstrate that as long as the MROI is reasonably close to the nose tip, its exact position and size do not significantly affect the computation.

VII. CONCLUSION

Breathing is a significant vital function. Breathing rate is used as an indicator of overall health and also in diagnosis of chronic or acute diseases, like obstructive sleep apnea or heart attack. In this paper we have described a method based on passive and contact-free sensing (thermal imaging) to measure breathing rate. The sensor used (thermal camera) can operate as a computer peripheral, and therefore, the method joins the suite of methods we have proposed previously for desktop health monitoring.

The present method operates in the CO_2 absorption band of MWIR that has as a result an improved Signal to Noise ratio (S/N) with respect to the MWIR method we reported in [9]. Also, in contrast to the statistical methodology we applied to compute breathing rate in [9], we apply a Fourier based method similar to the one we used to compute pulse in [8]. For the first time, however, we employ mutli-stage windowing on the FFT computation, which results in increased accuracy over the course of time. An Electronic Trigger (ET) renders the ground-truthing operation very reliable without any noticeable phase shift between the imaging and contact sensing modalities.

Overall, the performance of our current method is better than the one reported in [9]. In the future, we plan on im-

TABLE II

MROI SENSITIVITY ANALYSIS FOR CLIP D005-010

MROI	Stage 1		Stage 2		Stage 3	
	GBR	IBR	GBR	IBR	GBR	IBR
(a)	13.89	16.54	14.73	15.24	11.69	13.27
(b)	13.89	16.53	14.73	15.23	11.69	13.27
(c)	13.89	16.54	14.73	15.25	11.69	13.27
(d)	13.89	16.52	14.73	15.27	11.69	13.27

proving the tracking mechanism to cope with more agitated subjects. We also plan on addressing the issue of frontal view computation versus the current profile view - a more difficult problem due to the overwhelming effect of tissue radiation from the face.

ACKNOWLEDGMENT

We would like to thank the National Science Foundation (grant # IIS-0414754) and Dr. Ephraim Glinert, for their support and encouragement during the lifetime of this burgeoning research project. Equally, we would like to thank the Computer Science Department of the University of Houston for providing additional support. The views expressed by the authors in this paper do not necessarily reflect the views of the funding agencies.

REFERENCES

[1] F. H. Martini, W. C. Ober, C. W. Garrison, K. Welch, and R. T. Hutchings, *Fundamentals of Anatomy and Physiology*, ch. 23. Upper Saddle River, N.J.: Prentice Hall, 5th ed., 2001.

[2] S. Iamratanakul, J. McNames, and B. Goldstein, "Estimation of respiration from physiologic pressure signals," in *Proceedings of the 26th Annual International Conference of the IEEE Engineering in Medicine and Biology Society*, (San Francisco, CA), September 2004.

[3] J. McNames, J. Bassale, M. Aboy, C. Crespo, and B. Goldstein, "Techniques for the visualization of nonstationary biomedical signals," in *Proceedings of the 16th International EURASIP Conference BIOSIGNAL 2002*, vol. 16, (Brno, Czech Republic), pp. 42–45, 26-28 June 2002.

[4] J. McNames and A. Fraser, "Obstructive sleep apnea detection based on spectrogram patterns in the electrocardiogram," *Computers in Cardiology*, vol. 27, pp. 749–752, September 2000.

[5] ADInstruments, "2205 Executive Circle, Colorado Springs, Colorado 80906." http://www.adinstruments.com.

[6] E. Greneker, "Radar sensing of heartbeat and respiration at a distance with security applications," in *Proceedings of SPIE, Radar Sensor Technology II*, vol. 3066, (Orlando, Florida), pp. 22–27, April 1997.

[7] M. Garbey, A. Merla, and I. Pavlidis, "Estimation of blood flow speed and vessel location from thermal video," in *Proceedings of the IEEE Computer Society Conference on Computer Vision and Pattern Recognition*, (Washington, DC), June 27 - July 2 2004.

[8] N. Sun, M. Garbey, A. Merla, and I. Pavlidis, "Imaging the cardiovascular pulse," in *Proceedings of the IEEE Computer Society Conference on Computer Vision and Pattern Recognition*, (San Diego, CA), June 20-25 2005. to appear.

[9] R. Murthy, I. Pavlidis, and P. Tsiamyrtzis, "Touchless monitoring of breathing function," in *Proceedings of the 26th Annual International Conference IEEE Engineering in Medicine and Biology Society*, (San Fransisco, CA), September 2004.

[10] I. Pavlidis, "Continuous Physiological Monitoring," in *Proceedings of the 25th Annual International Conference of the IEEE Engineering in Medicine and Biology Society*, (Cancun, Mexico), September 17-21 2003.

[11] G. C. Holst, *Common Sense Approach to Thermal Imaging*, ch. 5. Bellingham, Washington: SPIE - The International Society for Optical Engineering, 2000.

[12] B. D. Lucas and T. Kanade, "An iterative image registration technique with an application to stereo vision," in *Proc 7th Intl Joint Conf on Artificial Intelligence (IJCAI)*, (Vancouver, British Columbia), pp. 674 –679, August 24-28 1981.

[13] J. Cooley and J. Tukey, "An algorithm for the machine computation of the complex Fourier series," *Mathematics of Computation*, vol. 19, pp. 297–301, April 1965.

[14] J. Mcnames, "Relationship of Fourier Transform and the FFT for Sampled Signals," Tech. Rep. 02-1, Portland State University, February 7 2002.

[15] Flir Systems - Indigo Operations, "70 Castilian Dr., Goleta, California 93117." http://www.indigosystems.com.

[16] QuickSet International Inc., "3650 Woodhead Drive, Northbrook, Illinois 60062." http://www.quickset.com.

[17] Santa Barbara Infrared Inc., "30 South Calle Cesar Chavez, Suite D, Santa Barbara, California 93103." http://www.sbir.com.

[18] Dell Inc., "One Dell Way, Round Rock, Texas, 78682." http://www.dell.com.

[19] Spectrogon Inc., "Subsidiary of Spectrogon AB, 24b Hill Rd., Parsippany, New Jersey 07054." http://www.spectrogon.com.

[20] K. Pearson, "Mathematical contributions to the theory of evolution III. Regression, heredity and panmixia," *Philosophical Transactions of the Royal Society of London*, vol. 187, pp. 253–318, 1896.